

Evolution of Compact-Binary Populations in Globular Clusters: A Boltzmann Study

II. Introducing Stochasticity

Sambaran Banerjee and Pranab Ghosh

*Department of Astronomy & Astrophysics
Tata Institute of Fundamental Research, Mumbai 400 005, India*

ABSTRACT

We continue exploration of the Boltzmann scheme started in Banerjee and Ghosh (2007, henceforth Paper I) for studying the evolution of compact-binary populations of globular clusters, introducing in this paper an explicit method for describing the inherent stochasticity of the dynamical processes of binary formation, destruction and hardening in globular clusters due to stellar encounters. We describe the fluctuations in the rates of the above stochastic processes as a *Wiener process*. The Boltzmann equation then becomes a stochastic partial differential equation, the solution of which involves the use of *Itô calculus* (this use being the first, to our knowledge, in this subject), in addition to ordinary calculus. As in Paper I, we focus on the evolution of (a) the number of X-ray sources N_{XB} in globular clusters, and (b) the orbital-period distribution of the X-ray binaries, showing explicitly the fluctuations in the results due to the stochasticity in the above processes. We show that, although the details of these fluctuations differ from one “realization” to another of the stochastic processes, the general trends of the full results follow those found in the continuous-limit study of Paper I. Indeed, the average result over many such realizations is very close to the continuous-limit result, showing the value of the latter for understanding overall trends. Extending the results of Paper I, we investigate the dependence of N_{XB} found by these full calculations on two essential globular-cluster properties, namely, the star-star and star-binary encounter-rate parameters Γ and γ , which we used extensively in Paper I, and which we called Verbunt parameters. We compare our computed results with those from CHANDRA observations of galactic globular clusters, showing that the expected scaling of N_{XB} with the Verbunt parameters is in good agreement with the observed one. We indicate how more complicated, time-dependent problems can be tackled with this scheme, and also what additional features are to be incorporated into the scheme in the future.

Subject headings: globular clusters: general— binaries: close — X-rays: binaries
— methods: numerical — stellar dynamics — scattering

1. Introduction

In this series of papers, we are studying the evolution of compact-binary populations of globular clusters with the aid of a Boltzmann scheme which we introduced in Banerjee & Ghosh (2007), henceforth Paper I. This scheme follows compact-binary evolution as a result of both (a) those processes which determine compact-binary evolution in isolation (*i.e.*, outside globular clusters), *e.g.*, angular momentum loss by gravitational radiation and magnetic braking, as also orbital evolution due to mass transfer, and (b) those processes which arise from encounters of compact binaries with the dense stellar background in globular clusters, *e.g.*, collisional hardening (Heggie 1975; Shull 1979; Banerjee & Ghosh 2006), binary formation through tidal capture and exchange processes, and binary destruction (Fabian et.al. 1975; Press & Teukolsky 1977; Lee & Ostriker 1986; Di Stefano & Rappaport 1992, 1994; Spitzer 1987; Hut & Bahcall 1983). We treat all of the above processes simultaneously through our Boltzmann scheme, the aim being to see their combined effect on the compact-binary population as a whole, in particular on the evolution of (a) the total number of X-ray binaries as the formation and destruction processes continue to operate, and, (b) the orbital-period distribution of the population. As stressed in Paper I, our scheme is the original Boltzmann one (not the Fokker-Planck reduction of it), which, by definition, is capable of handling both the *combined* small effects of a large number of frequent, weak, distant encounters and the *individual* large effects of a small number of rare, strong, close encounters *on the same footing*. We note here that, although Monte Carlo Fokker-Planck approaches were normally thought to be capable of handling only the former effects, schemes for including the latter have been proposed and studied recently (Fregeau et.al 2003; Fregeau & Rasio 2007).

In Paper I, we studied the problem in the continuous limit, wherein we used continuous representations for both kinds of processes described above, *i.e.*, those of category (a) above, which are inherently continuous, and also those of category (b), which are inherently stochastic. For the latter category, therefore, we used the *continuous limit* of the above stochastic processes, wherein the probability or cross-section of a particular such process happening with a given set of input and output variables was treated as a continuous function of these variables. These cross-sections were, of course, those that had been determined from extensive numerical experiments with two-body and three-body encounters performed earlier (Heggie, Hut & McMillan 1996; Portegies Zwart et.al 1997b).

In this paper, we address the next question, namely, how is the inherent stochasticity of the processes of category (b) to be introduced into our scheme, to be handled simultaneously with the inherently continuous nature of those of category (a)? As stressed in Paper I, this step is of great importance, since it is a simultaneous operation of the above continuous and stochastic processes in globular clusters that leads to the observed properties of compact-binary populations in them. To this end, we introduce stochasticity into our Boltzmann study in this paper in the following way. For a first look, we consider the rates of the processes of category (b) as *randomly fluctuating* about the mean rates described in Paper I, while those of the processes of category (a) remain continuous, as before. We model these fluctuations as a *Wiener process* (see Appendix A and references therein), which is the mathematical description of Brownian motion.

With this prescription, the Boltzmann equation governing the evolution of the distribution function $n(a, t)$ of compact binaries in time t and orbital radius a becomes a *stochastic* partial differential equation (henceforth SPDE), instead of the ordinary partial differential equation (henceforth OPDE) which it was in the continuous limit. We handle the solution of this SPDE with the aid of techniques developed largely during the last fifteen years (Kloeden et.al 1994; Gains 1995; Øksendal 2004). These techniques involve the use of the *Itô calculus* (see Appendix B and references therein), instead of ordinary calculus, for handling the stochastic terms.

Our results show that the full solutions with stochasticity included have fluctuations which vary from one “realization” to another of the stochastic processes, as expected. However, the full results show trends which generally follow those in the continuous limit. Furthermore, the average result over many realizations comes very close to the continuous limit, showing the importance of the latter limit for understanding mean trends. On the other hand, understanding fluctuations in a typical full run is also very important, as this gives us a first idea of the magnitude of fluctuations we can expect in the data on X-ray binaries in globular clusters as a result of the stochastic processes, as also the expected trends in the fluctuations with the essential globular-cluster parameters, *e.g.*, the Verbunt parameters introduced in Paper I (also see below).

Comparison of our computed trends in the number N_{XB} of X-ray binaries in Galactic globular clusters with the Verbunt parameters on the one hand, with observed trends in recent CHANDRA data on Galactic globular clusters on the other, shows that our full results are in good agreement with observation. We have thus constructed a straightforward, very inexpensive scheme for following the evolution of compact-binary populations in globular clusters, including essential, fluctuating, encounter processes that are thought to operate in such clusters, as also those continuous processes which operate in isolated binaries and so

apply here as well. We can also follow the evolution of N_{XB} , as also that of the orbital-period distribution of compact binaries in globular clusters. For the latter study, however, proper modeling of stellar-evolutionary effects still remains to be done for parts of the parameter space, as explained in Paper I, and as discussed in Sec. 5.

In Sec. 2, we briefly review the continuous-limit results of Paper I, in order to put the results of this paper in their proper context. We give only the essentials here, citing figures in Paper I for detailed results. In Sec. 3, we introduce stochasticity explicitly through our prescription, explaining the details of Wiener processes and the Itô calculus in the Appendices. We describe our generalization of the Lax-Wendroff scheme, introduced in Paper I, to handle the solution of the SPDE which the Boltzmann equation has become now. In Sec. 4, we describe the results of our full calculations including stochasticity, and compare these with the continuous-limit results of Paper I. In Sec. 4.3, we compare our full results with observations. Finally, In Sec. 5, we discuss our results, putting them in the context of previous studies in the subject, and indicating some additional physical effects to be included by stages in future versions of our scheme, as well as some future problems to be tackled.

2. Brief Review of Continuous Limit

In order to put the stochastic studies of this paper in their proper context, we review in this section the essentials of the continuous-limit studies of Paper I which form this context. In the latter limit, the Boltzmann description works in terms of appropriate *mean* values of the variables and parameters which are actually stochastic. Accordingly, the above compact-binary distribution function $n(a, t)$ is replaced by its mean value $\bar{n}(a, t)$, and the Boltzmann equation has the form:

$$\frac{\partial \bar{n}(a, t)}{\partial t} = \bar{R}(a) - \bar{n}(a, t)\bar{D}(a) - \frac{\partial \bar{n}(a, t)}{\partial a}\bar{f}(a). \quad (1)$$

Here, $\bar{R}(a)$ is the mean formation rate (per unit binary radius) of compact binaries of radius a , $\bar{D}(a)$ is the mean destruction rate per binary and $\bar{f}(a)$ is the mean shrinkage rate \dot{a} of a compact binary of radius a , as described in Paper I.

2.1. Mean rates

The mean shrinkage or “hardening” rate $\bar{f}(a) = \dot{a}$ has been given in Fig. 2 of Paper I as a function of a , describing the situation as the compact binary goes from its widest, pre-X-

ray-binary (PXB) phase to Roche lobe contact, and continues through the mass-transferring X-ray-binary (XB) phase. As shown there, collisional hardening, *i.e.*, that due to encounters between the binary and the stellar background of the globular cluster, dominates at large a , while hardening by gravitational radiation and magnetic braking dominates at small a . The relative orbit shrinkage rate \dot{a}/a scales roughly as a at large orbital radii, passes through a minimum at a critical separation where the gravitational radiation shrinkage rate, scaling as $\dot{a}/a \sim a^{-4}$, takes over. Magnetic braking also contributes at small radii, but Roche lobe contact also occurs at roughly the same point, whereupon the angular-momentum transfer associated with mass transfer in the XB phase dominates the orbit-change rate, and \dot{a} has a very weak dependence on a during this phase. Detailed quantitative expressions for the above rates are given in Paper I, to which we refer the reader, recording here only that the orbit-shrinkage rate is given in terms of the angular-momentum loss rate by

$$\frac{\dot{a}}{a} = 2\frac{\dot{J}}{J} - 2\frac{\dot{m}_c}{m_c} - 2\frac{\dot{m}_X}{m_X}, \quad (2)$$

where m_X is mass of the degenerate star in the compact binary, and m_c is that of its (low-mass) companion, and the total angular-momentum loss rate can be written in terms of its components as:

$$j(a) \equiv \frac{\dot{J}}{J} = j_{GW}(a) + j_{MB}(a) + j_{coll}(a). \quad (3)$$

Here, the subscripts ‘GW’, ‘MB’ and ‘coll’ respectively stand for gravitational radiation, magnetic braking, and collisional hardening.

The other essential mean rates are those of compact binary formation and destruction, $\overline{R}(a)$ and $\overline{D}(a)$, respectively. Consider first the formation of compact binaries with degenerate primaries (white dwarfs or neutron stars) and low-mass companions, such as we are interested in this series of papers, in globular cluster (henceforth GC) cores. The two relevant dynamical processes are (i) tidal capture (tc) of a degenerate, compact star by an ordinary, low-mass star, and (ii) an exchange encounter (ex1) between such a compact star and a binary of two ordinary low-mass stars in the GC, wherein the compact star replaces one of the binary members. Accordingly, the total mean rate of formation of compact binaries per unit binary radius, $\overline{R}(a)$, consists of the above mean tc rate $r_{tc}(a)$ and mean ex1 rate $r_{ex1}(a)$:

$$\overline{R}(a) = r_{tc}(a) + r_{ex1}(a). \quad (4)$$

The above mean rates are shown as functions of a in Fig. 3 of Paper I, and detailed mathematical expressions for them are also given in that reference, which we do not repeat here. The mean tidal-capture rate is nearly constant for $a < 5R_\odot$, and decreases rapidly at larger a . Extensive discussion of various issues related to tidal capture and of the current status

of our understanding of this process are also given in Paper I, to which we refer the reader. Further discussion of previous studies of tidal capture in this problem are given in Sec. 5. The mean exchange (ex1) rate is roughly constant over the range of radii of interest here, for the widely-adopted radius distribution of primordial binaries, *viz.*, a uniform distribution in $\ln a$, which we adopt throughout our work.

Consider now the destruction of compact binaries with degenerate primaries and low-mass companions, which can occur in the following two ways. First, an encounter with a star which has a relative speed higher than an appropriate critical speed can lead to its dissociation (dss). Second, in an exchange encounter (ex2) of this binary with a compact star, the latter can replace the low-mass companion in the binary, forming a double compact-star binary consisting of two neutron stars, two white dwarfs, or a neutron star and a white dwarf (all with masses $m_X \approx 1.4M_\odot$ in our model: see Paper I). This destroys the binary as an X-ray source (as accretion is not possible in such a system), and so takes it out of reckoning in our study¹. The total mean destruction rate $\overline{D}(a)$ *per binary* is thus the sum of the above mean dss and ex2 rates:

$$\overline{D}(a) = r_{ex2}(a) + r_{dss}(a) \quad (5)$$

The above mean rates are shown as functions of a in Fig. 3 of Paper I, and detailed mathematical expressions for them are given in that paper, which, once again, we do not repeat here. The mean dissociation rate is negligible below a critical radius a_c corresponding to the above critical speed, rises extremely sharply above a_c at first, and eventually scales as a^2 for $a \gg a_c$. By contrast, the mean exchange (ex2) rate is roughly $\propto a$ and dominates the destruction processes completely at all orbital radii relevant to our study, dissociation becoming important only for very soft binaries ($a > 1000R_\odot$, say), which are of little interest to us here.

2.2. Results

We now summarize the essentials of our continuous-limit results in Paper I. We computed evolution of the compact-binary distribution in this limit, showing the surface $n(a, t)$ explicitly in three dimensions in Fig. 5 of Paper I, corresponding to representative GC parameters (rather similar to those of the well-known Galactic cluster 47 Tuc). The surface

¹Note that it is essentially impossible for one of the compact stars in such a double-compact system to be re-exchanged with an ordinary star in a subsequent exchange encounter, since the average mass of a background GC star (taken as $m_f = 0.6M_\odot$ in our work) is much less than the above value of m_X .

evolved smoothly, with the compact-binary population growing predominantly at shorter radii ($a < 10R_\odot$, say). We showed that, starting with a small number of binaries at $t = 0$ following various distributions, we obtained at times \sim Gyr or longer a distribution which was independent of the initial conditions, determined entirely by the dynamical processes of formation and destruction, and by the various hardening processes summarized above. We clarified the nature of the distribution and its evolution by displaying slices through the above surface at various points along time axis and a -axis, shown in Figs. 6 and 7 of Paper I. The former figure showed that the profile $n(a)$ increased with time, roughly preserving its profile for $t > 1.5$ Gyr, this profile consisting of a roughly uniform distribution at small orbital radii, $a \leq 6R_\odot$, say, and a sharp fall-off at larger radii. The latter figure showed that $n(a)$ at a given a increased with time and approached saturation on a timescale $6 - 12$ Gyr, the timescale being longer at smaller values of a .

For comparison with crucial X-ray observations of Galactic GCs, we computed the total number of XBs N_{XB} in a GC at any time, obtained by integrating $n(a, t)$ over the range of a relevant for XBs, *viz.*, $a_{pm} \leq a \leq a_L$, where a_{pm} is the value of a corresponding to the period minimum $P \approx 80$ minutes, and a_L is the value of a at the first Roche lobe contact and onset of mass transfer, as explained above:

$$N_{XB}(t) = \int_{a_{pm}}^{a_L} n(a, t) da. \quad (6)$$

Taking an evolutionary time ~ 8 Gyr as representative, we determined N_{XB} at this point in time, and studied its dependence on the Verbunt parameters Γ and γ that describe the essential dynamical properties of globular clusters in this context, as explained in Paper I, showing our results as the computed $N_{XB}(\Gamma, \gamma)$ surface in three dimensions in Fig. 8 of that paper.

The Verbunt parameters Γ and γ have been introduced in Paper I. Following pioneering suggestions by Verbunt and co-authors (Verbunt & Hut 1987; Verbunt et.al 1989), the crucial importance of these parameters in GC dynamics has been lucidly summarized recently by Verbunt (Verbunt 2003, 2006), and the importance of the parameter Γ for scaling between different GCs has been emphasized in a pioneering study of the production of recycled pulsars in GCs by Di Stefano & Rappaport (1992). Briefly, the first parameter Γ is the two-body stellar encounter rate, which scales with $\rho^2 r_c^3 / v_c$, and occurs naturally in the rates of all two-body processes, where the standard GC core variables are the average stellar density ρ , the velocity dispersion v_c , and the core radius r_c . In fact, we defined Γ as

$$\Gamma \equiv \frac{\rho^2 r_c^3}{v_c} \propto \rho^{3/2} r_c^2, \quad (7)$$

in Paper I. Note that the last scaling in the above equation holds only for virialized cores,

where the scaling $v_c \propto \rho^{1/2} r_c$ can be applied. The second parameter is a measure of the rate of encounter between binaries and single stars in the GC, the rate normally used being the encounter rate γ of a *single* binary with the stellar background, with the understanding that the total rate of binary-single star encounter in the cluster will be $\propto n\gamma$. We defined γ in Paper I as

$$\gamma \equiv \frac{\rho}{v_c} \propto \rho^{1/2} r_c^{-1}, \quad (8)$$

where the last scaling holds, again, only for virialized cores.

We compared the results of our above computations with the systematics of recent observations of X-ray binaries in Galactic globular clusters (Pooley et.al 2003), as displayed in Figs. 9 and 10 of Paper I. We showed that the computed total number N_{XB} of XBs expected in a globular cluster scaled in a characteristic way with the Verbunt parameters. The qualitative nature of this scaling was rather similar to that found in our earlier “toy” model (Banerjee & Ghosh 2006), although details were different. N_{XB} scaled with Γ (which is a measure of the dynamical formation rate of compact binaries, as above) and, at a given Γ , N_{XB} decreased with increasing γ (which is a measure of the rate of destruction of these binaries by dynamical processes) at large values of γ , as shown in Fig. 9 of Paper I. This rough scaling could be expressed as $N_{XB} \propto \Gamma g(\gamma)$, where the “universal” function $g(\gamma)$ of γ (except for a spurious feature at low values of γ which we explained in Paper I) decreased monotonically with increasing γ , reflecting the increasing strength of dynamical binary-destruction processes with increasing γ .

We further demonstrated that these computed trends with the Verbunt parameters compared very well with the observed trends in above X-ray data by showing in Fig. 10 of Paper I the contours of constant N_{XB} in the $\Gamma - \gamma$ plane, and overplotting on the positions of the Galactic GCs with observed X-ray binaries in them. We showed that the trend in the observed N_{XB} values generally followed the contours, with one exception. This provided us with a first indication of the basic ways in which dynamical binary formation and destruction processes work in GCs, and encouraged us to build more “realistic” models by introducing stochastic effects explicitly, to which this paper is devoted.

3. Introducing Stochasticity

In order to study the behavior of the inherently stochastic terms in the full Boltzmann equation

$$\frac{\partial n(a, t)}{\partial t} = R(a, t) - n(a, t)D(a, t) - \frac{\partial n(a, t)}{\partial a} f(a, t), \quad (9)$$

we must explicitly include stochastic, fluctuating parts in these terms, in addition to their mean values studied in Paper I, as above. We do so by expressing the above rates $R(a, t)$, $D(a, t)$, and $f(a, t)$ as their earlier mean values $\overline{R}(a)$, $\overline{D}(a)$ and $\overline{f}(a)$, augmented by fluctuating components as below:

$$\left. \begin{aligned} R(a, t) &= \overline{R}(a) + \zeta_{atc}^t + \zeta_{aex1}^t \\ D(a, t) &= \overline{D}(a) + \zeta_{aex2}^t + \zeta_{adss}^t \\ f(a, t) &= \overline{f}(a) + \zeta_{acoll}^t \end{aligned} \right\} \quad (10)$$

Here, ζ_{aX}^t is the random fluctuation rate of events of type X from their mean rates, and X = tc, ex1, ex2, dss, coll by turn, these notations having been introduced above. In general, ζ_{aX}^t is a function of both a and t , of course.

The crucial question is that of modeling ζ_{aX}^t appropriately. In this introductory work, we use the standard normally-distributed model

$$\zeta_{aX}^t = S_X(a)\eta^t, \quad (11)$$

where $S_X^2(a)$ is the variance of ζ_{aX}^t at a given a and η^t s at each t are independent random numbers distributed in a standard normal distribution. This separable form is appropriate since the dynamical processes of binary formation and destruction at a given value of a are inherently independent of those at other values of a . The “flow” or “current” of binaries from larger to smaller values of a due to the hardening described above and in Paper I does not affect this independence, but merely changes the number of binaries in an infinitesimal interval of a around a given value of a at a given instant t , which is automatically taken into account by the Boltzmann equation (also see below). Indeed, the hardening process itself has this independence, *viz.*, that its rate at a given value of a is independent of that at other values of a , and so is separable in the same way. By contrast, the number distribution $n(a, t)$ of the binaries *cannot* be written in this form, since, at a particular a , it is determined both by the binary formation and destruction rates at that a , *and* by the rates of binary arrival from (and also departure to) other values of a due to hardening, as described above. All of this is, of course, automatically included in the Boltzmann equation by definition.

The essence of the physics of these fluctuations is contained in the adopted model for η^t . By adopting a normally-distributed variation, we are, in effect, considering a *Wiener process* (see Appendix A and references therein), which is the standard mathematical description of Brownian motion. In other words, we are studying a situation wherein the variations in the above dynamical rates about their respective mean values constitute a Brownian motion. We return to Wiener processes later in more detail.

3.1. Variances of stochastic-process rates

How do we estimate the variance of a stochastic process of type X whose mean value is $\overline{R}_X(a)$? To answer this question, consider first how it is addressed in Monte Carlo simulations, which have been performed in this subject by several authors (see, *e.g.*, Sigurdsson & Phinney (1993), Portegies Zwart et.al (1997a), or Fregeau et.al (2003)). These works have uniformly used the so-called *rejection method* for determining whether an event of a given type occurs in a given time interval or not. The method works as follows.

For events of type X, if the mean rate of event occurrence is \overline{R}_X , then the timescale for occurrence of such events is

$$\Delta t_X = \frac{1}{\overline{R}_X} \quad (12)$$

Hence, during a time step $\Delta t < \Delta t_X$, the quantity $p_X = \overline{R}_X \Delta t < 1$ is the *expected mean number of events* during this interval. $p_X < 1$ can also be interpreted as the *probability* of occurrence of an event X within this time step (Portegies Zwart et.al 1997a), and the actual number of such events within Δt will then follow a binomial distribution with the following mean and variance:

$$\left. \begin{aligned} \text{mean} &= \overline{R}_X(a) \Delta t \\ \text{variance} &= S_X^2(a) \Delta t^2 = \overline{R}_X(a) \Delta t (1 - \overline{R}_X(a) \Delta t). \end{aligned} \right\} \quad (13)$$

Note that the above variance depends on a , since the mean rates depend on a . When several different types of events are considered simultaneously, as in the present problem, we must, of course, so choose Δt that it is shorter than the shortest event-occurrence timescale appearing in the problem. We discuss this point below.

3.1.1. Time step

The mean rates depend on a as detailed in Paper I (see Fig. 3 of that paper). $\overline{R}_{tc}(a)$ is a decreasing function of a , and so attains its maximum at $a = a_{min}$. All other rates are either constant (ex2), or increasing functions of a , so that their maximum values can be thought to occur at $a = a_{max}$. Accordingly, if we make the following choice for our computational time step Δt_d :

$$\Delta t_d < \min \left\{ \frac{1}{\overline{R}_{tc}(a_{min})}, \frac{1}{\overline{R}_{ex1}(a_{max})}, \frac{1}{\overline{R}_{ex2}(a_{max})}, \frac{1}{\overline{R}_{dss}(a_{max})}, \frac{1}{\overline{a}_{coll}(a_{max})} \right\}, \quad (14)$$

this will ensure that Δt_d is smaller than the shortest of the above event-occurrence timescales.

However, as is well-known, this time step must also obey the *Courant condition* (Press et.al 1992) throughout the range of a under consideration (*i.e.*, $0.6R_{\odot}$ - $60R_{\odot}$):

$$\Delta t_c = \epsilon \frac{\Delta a}{\bar{f}_{\max}}, \quad \epsilon < 1. \quad (15)$$

Here, Δa is the step-size in a , and \bar{f}_{\max} is the largest value of $\bar{f}(a)$ over the range of a under consideration (see above and paper I). Satisfaction of this condition is essential for the stability (Press et.al 1992) of the solution of Eqn. (9).

To ensure that both of the above conditions are satisfied, we choose the time step Δt for solving Eqn. (9) to be

$$\Delta t = \min\{\Delta t_d, \Delta t_c\}. \quad (16)$$

3.2. Solution of Stochastic Boltzmann Equation

The Lax-Wendorff scheme (Press et.al 1992) used by us for numerical solution of the Boltzmann equation in the continuous limit has been introduced in Sec. 2.6 of Paper I. The stochastic version of this equation, *viz.*, Eqn. (9) can be looked upon as the earlier continuous equation with additional stochastic terms, which turns it into a SPDE (see Sec. 1). We now discuss our method of solving this SPDE².

It is well-known that ordinary calculus cannot be applied to the handling of stochastic terms in SPDEs, since these terms are non-differentiable in the ordinary sense, and the ordinary definition of an integral does not apply to them. Rather, one has to modify the methods of calculus suitably, and redefine appropriate integrals. As summarized in Appendix B, one such modified calculus is the *Itô Calculus*, which has been used widely for solution of SPDEs in recent years (Øksendal 2004; Kloeden et.al 1994). The corresponding integrals involving the stochastic terms are then called *Itô integrals*, which have properties appropriately different from those of ordinary integrals, as indicated in Appendix B.

²In SPDE literature, the continuous terms are sometimes called *drift* terms and the stochastic terms *diffusion* terms, but we shall *not* use this terminology here, since stochastic terms in our problem do not always represent diffusion, and furthermore since there is a possibility with such usage of confusion with the Fokker-Planck approach, which does represent diffusion in phase space.

3.2.1. Numerical Method

In solving an SPDE like Eqn. (9), one integrates the continuous terms in the usual way, but the stochastic terms must be integrated using Itô calculus (Gains 1995). This means that, in advancing the solution at t by a time step dt — which is essentially a Taylor expansion of the solution $n(a, t)$ about t — the expansions of the stochastic terms in Eqn. (9) are to be performed using the stochastic Taylor expansion (Eqn. (B7)), as discussed in Appendix B.

A variety of numerical algorithms have been explored by various authors for numerical solution of SPDEs. The particular algorithm we use is a hybridization of the two-step Lax-Wendorff scheme for the continuous terms, as utilized in paper I, and the second-order stochastic Taylor expansion according to the *Milshtein scheme* for the stochastic terms (Milshtein 1974; Gains 1995), *i.e.*, Eqn. (B13), as explained in Appendix B. In this scheme, there is only one stochastic path to be solved for in our case *viz.*, that of $n(a, t)$ (corresponding to X_k) and the continuous terms (*i.e.*, the σ_{ps}), the variances in tc, ex1, ex2, dss and coll rates being as given above. Note that, in each of the two steps in the Lax-Wendorff scheme, the expansion (B13) needs to be applied, whereupon we arrive at the following discretization scheme³ for Eqn. (9):

$$\begin{aligned}
 &\text{Half step :} \\
 n_{j+1/2}^{N+1/2} &= \frac{1}{2} (n_{j+1}^N + n_j^N) + \left[\bar{R}(a_{j+1/2}) - \bar{D}(a_{j+1/2}) \left(\frac{n_{j+1}^N + n_j^N}{2} \right) \right] \frac{\Delta t}{2} \\
 &+ \left(\mathcal{W}_{j+1/2}^N{}_{tc} + \mathcal{W}_{j+1/2}^N{}_{ex1} \right) - \left(\mathcal{W}_{j+1/2}^N{}_{ex2} + \mathcal{W}_{j+1/2}^N{}_{dss} \right) \left(\frac{n_{j+1}^N + n_j^N}{2} \right) \\
 &+ \left[\left((\mathcal{W}_{j+1/2}^N{}_{ex2})^2 - S_{ex2}^2(a_{j+1/2}) \right) + \left((\mathcal{W}_{j+1/2}^N{}_{dss})^2 - S_{dss}^2(a_{j+1/2}) \right) \right] \left(\frac{n_{j+1}^N + n_j^N}{4} \right) \\
 &+ \left(\mathcal{W}_{j+1/2}^N{}_{ex2} \mathcal{W}_{j+1/2}^N{}_{dss} \right) \left(\frac{n_{j+1}^N + n_j^N}{2} \right) \\
 &- \frac{\bar{f}(a_{j+1/2})\Delta t}{2\Delta a} (n_{j+1}^N - n_j^N) - \frac{\mathcal{W}_{j+1/2}^N{}_{coll}}{2\Delta a} (n_{j+1}^N - n_j^N), \tag{17}
 \end{aligned}$$

$$\begin{aligned}
 &\text{Full step :} \\
 n_j^{N+1} &= n_j^N + (\bar{R}(a_j) - \bar{D}(a_j) n_j^N) \Delta t \\
 &+ \left(\mathcal{W}_j^N{}_{tc} + \mathcal{W}_j^N{}_{ex1} \right) - \left(\mathcal{W}_j^N{}_{ex2} + \mathcal{W}_j^N{}_{dss} \right) n_j^N \\
 &+ \left[\left((\mathcal{W}_j^N{}_{ex2})^2 - S_{ex2}^2(a_j) \right) + \left((\mathcal{W}_j^N{}_{dss})^2 - S_{dss}^2(a_j) \right) \right] \frac{n_j^N}{2} \\
 &+ \left(\mathcal{W}_j^N{}_{ex2} \mathcal{W}_j^N{}_{dss} \right) n_j^N \\
 &- \frac{\bar{f}(a_j)\Delta t}{\Delta a} \left(n_{j+1/2}^{N+1/2} - n_{j-1/2}^{N+1/2} \right) - \frac{\mathcal{W}_j^N{}_{coll}}{\Delta a} \left(n_{j+1/2}^{N+1/2} - n_{j-1/2}^{N+1/2} \right).
 \end{aligned}$$

Here, $\mathcal{W}_j^N{}_X \equiv S_X(a_j)\eta^N\Delta t$, where η^N is the value of a standard normal variate at the N th time step.

³It can be shown that the commutation condition (B15) is satisfied in this case.

For any particular run, we compute the $\mathcal{W}_{j\ X}^N$ ($\mathcal{W}_{j+1/2\ X}^N$ s) for a particular a_j ($a_{j+1/2}$) over the a and t intervals of integration, and repeat it for all a_j s. The standard normal variate η^N s are generated using the well-known *polar method* (Press et.al 1992). All values of $\mathcal{W}_{j\ X}^N$ and $\mathcal{W}_{j+1/2\ X}^N$ are stored in a two dimensional array (*i.e.*, a *Wiener sheet*), which serves as the input for solving Eqn. (17). Because of the fluctuations in the collisional hardening rate (as contained in $\zeta_{a\ coll}^t$), it is not impossible that the value of the total hardening rate f might occasionally exceed \bar{f}_{max} , which would violate the Courant condition, possibly making the solution procedure unstable. To avoid this, we have so restricted the variations in $\mathcal{W}_{j\ coll}^N$ s and $\mathcal{W}_{j+1/2\ coll}^N$ s that the *amplification factor* $\epsilon \equiv f\Delta t/\Delta a$ always lies between zero and unity (Press et.al 1992).

4. Results

We now present the results obtained from our above computations of the cases which we studied in Paper I in the continuous limit. As before, we study (a) the evolution of the distribution function $n(a, t)$, and, (b) the dependence of the computed number of XBs N_{XB} on the Verbunt parameters. We choose exactly the same values of all GC parameters as we did in Paper I, for ease of comparison.

4.1. Evolution of compact-binary distribution

In Fig. 1, we show a typical evolution of the compact binary population distribution $n(a, t)$. The GC parameters were chosen, as in Paper I, to be $\rho = 6.4 \times 10^4 M_\odot \text{pc}^{-3}$, $r_c = 0.5 \text{ pc}$ and $v = 11.6 \text{ km sec}^{-1}$, similar to those of the well-known Galactic cluster 47 Tuc. As the figure shows, the surface representing the evolution fluctuates randomly throughout, but it does show a clear overall evolution which is of the same nature as that in the continuous limit (cf. Fig. 5 of Paper I). In particular, the population grows with time predominantly at shorter radii ($a < 10R_\odot$). As before, we start with a small number of primordial compact binaries with various initial distributions, and find that, by $t \sim 1 - 1.5 \text{ Gyr}$, the distribution “heals” to a form which is independent of the initial choice of distribution. The fluctuations differ in detail from run to run, of course, as we choose different seeds for random number generation, but the overall nature of the evolution remains the same for all runs. Indeed, the results for different runs seem to represent different variations about a *mean* surface, which is very close to that in the continuous limit, as given in Paper I. We explicitly demonstrate this below by displaying temporal and radial slices through the above surface $n(a, t)$ (see Paper I) for different runs, and also displaying their averages over a number of runs, which

we show to be close to the continuous limit.

To do this, we first show in Fig. 2 typical time slices, *i.e.*, $n(a)$ at fixed t , (solid lines) through the surface in Fig. 1, for a *single* run, overplotting the continuous limit from Paper I for comparison. The distribution with fluctuations does indeed follow the continuous-limit distribution generally, the same gross features being visible through fluctuations, in particular that $n(a)$ is roughly constant $a \leq 7R_\odot$, and falls off sharply at larger radii. The overall nearly-self-similar evolution at large times, described in Paper I, can also be vaguely discerned through the fluctuations. We have discussed possible causes of such self-similar evolution in Paper I. Next, in Fig. 3, we show radial slices corresponding to the evolution in Fig. 1, representing the behavior of $n(t)$ at a fixed radius a , overplotted with the continuous limit from Paper I. Again, the curves from a single run follow, in a statistical sense, the corresponding continuous limits. In particular, it can be seen that the radial slices corresponding to larger values of a tend to saturate by about 6 Gyr, while those for smaller values of a do not show such saturation.

Finally, in Figs. 4 and 5, we show the above temporal and radial slices of the average of 12 different runs, overplotted with the the corresponding continuous limits. These figures clearly demonstrate how the fluctuations average out over many runs, so that the mean result approaches the continuous limit.

4.2. Number of X-ray binaries

The total number of GC X-ray binaries N_{XB} at a particular time was computed from Eq. (6), as in Paper I. We determined N_{XB} for a representative evolution time of ~ 8 Gyr, and studied its dependence on the Verbunt parameters Γ and γ , so as to relate our computational results with the systematics of recent observations of X-ray binaries in globular clusters (Pooley et.al 2003). For this, we computed, as in Paper I, values of N_{XB} over a rectangular grid in $\Gamma - \gamma$ space, spanning the range $\gamma = 1 - 10^6$ and $\Gamma = 10^3 - 10^8$, which encompasses the entire range of Verbunt parameters over which Galactic GCs have been observed (see Paper I). Although the GCs actually observed so far lie along a diagonal patch over this grid, as explained in Paper I, computational results over the whole grid are useful for clarifying the theoretically expected trends.

As explained in Paper I, at a specific grid point (Γ, γ) , the values of ρ , r_c and v_c are evaluated using the definitions of Verbunt parameters and the virialization condition (see Sec. 3.2 of paper I for a detailed discussion). Also as before, we take representative values of primordial stellar binary fraction (k_b) and compact-star fraction (k_X) to be 10 percent and

5 percent respectively.

Fig. 6 shows the resulting $N_{XB}(\Gamma, \gamma)$ surface. As indicated in Paper I, the overall fall-off in this surface for $\gamma > 3 \times 10^3$ is a signature of the increasing rates of compact-binary destruction rates with increasing γ , and the above specific value of γ represents an estimate of the threshold above which destruction rates are very important. Further, the trend in N_{XB} with Γ is simple — N_{XB} increases with Γ monotonically, since the dynamical formation rate of compact binaries scales with Γ . What we notice in fig. 6 is that this surface also shows random fluctuations due to the stochastic processes, but it generally follows the N_{XB} surface corresponding to the continuous limit, shown overplotted in the same figure. This is similar to what was discussed above for the compact-binary distribution, and the point about the mean surface corresponding to the average of many realizations of the stochastic processes being very close to the continuous limit also holds here. We also note that the *total* fluctuations in N_{XB} increase with increasing value of Γ . However, as will become evident from results discussed below, the *relative* fluctuations actually decrease with increasing Γ .

To further clarify the trends and to make comparisons with the results of the “toy” model of B06 and with those of Paper I, we plot the quantity Γ/N_{XB} for a *fixed* value of Γ against γ in Fig. 7, displaying the curves for several values of Γ as indicated. As can be seen, the fluctuating Γ/N_{XB} vs. γ curves for various values of Γ follow the same mean trend, although the details of the fluctuation are different in different cases. This mean trend is in fact very close to the mean “universal” curve corresponding in the continuous limit evolution of Paper I, and is overplotted in the figure. Thus, as in the continuous limit case, the basic scaling of the toy model, *viz.*, $N_{XB} \propto \Gamma g(\gamma)$, where $g(\gamma)$ is a “universal” decreasing function (representing the increasing binary destruction rate with increasing γ , as explained above), does essentially carry over to this detailed model with stochasticity included, suggesting a robust feature of the scaling between different clusters which is expected to be further confirmed by future observations.

Another feature of Fig. 7 is that the relative fluctuations in the curves increase with decreasing value of Γ . This is consistent with the intuitive notion that, in all phenomena of this nature, the relative fluctuations in N_{XB} are expected to increase at smaller values of N_{XB} , which occur at smaller values of Γ . More formally, this can be seen as follows. From Eqn. (13), it is clear that, over an interval Δt , the relative variance in the number of events of type X is:

$$r_X(a) = (1 - \overline{R}_X(a)\Delta t).$$

For the range of Γ and γ considered in this work, we found that Δt was actually close to Δt_c in most cases, so that $\Delta t \sim \gamma^{-1}$ roughly. Since the formation rates scale as $R_X \sim \Gamma$, we

have:

$$r_X(a) = \left(1 - \mathcal{O}\frac{\Gamma}{\gamma}\right).$$

Therefore, for a fixed γ , $r_X(a)$ increases as Γ (and hence N_{XB}) decreases.

4.3. Comparison with observations

In Secs. 4.1 and 4.2 we saw that the basic trends of the results, as obtained from the stochastic Boltzmann equation (9), are the same as those obtained from the Boltzmann equation in the continuous limit in Paper I. Therefore, as in paper I, the results from the stochastic Boltzmann equation are consistent with the observations of XB populations in Galactic GCs. Indeed, since fluctuations *are* present in the dynamical processes under study here, we should ideally compare theoretical trends including fluctuations with observational results, as we do in this paper, where Fig. 6 shows the positions of the observed GCs with significant numbers of X-ray sources in the $\gamma - \Gamma - N_{XB}$ co-ordinates. The observational points do lie near the computed $N_{XB}(\gamma, \Gamma)$ surface. In Fig. 7, we compare the $\Gamma/N_{XB} - \gamma$ curves with the positions of the observed points, showing that most points do indeed lie near the curves.

In Fig. 8 we plot the computed contours of constant N_{XB} in the plane of Verbunt parameters, similar to what we did in Fig. 10 of Paper I, but now with the fluctuations included. The fluctuations are clearly seen to be larger for smaller values of N_{XB} , as expected, and as mentioned above. Again, the observed numbers generally agree well with the present contours which include fluctuations, and these contours do generally follow the continuous-limit contours of Paper I, which are shown overplotted.

5. Discussions

We have described in this paper a scheme for introducing stochasticity into the Boltzmann study of compact-binary evolution in globular clusters that we began in Paper I. Our scheme involves the use of stochastic calculus (for the first time in this subject, to the best of our knowledge), whereas previous studies in the subject have normally used Monte-Carlo methods of various descriptions — depending on the particular aspect of the problem being studied — for handling stochasticity (see, *e.g.*, Hut, McMillan & Romani (1992); Di Stefano & Rappaport (1994); Fregeau et.al (2003); Fregeau & Rasio (2007)). With the aid of this scheme, we have demonstrated that the joint action of inherently stochastic and continuous processes produces evolutionary trends which necessarily contain fluctuations

that vary between individual “realizations” of the stochastic processes, as expected. However, these trends do generally follow those found in the continuous-limit approximation of Paper I, and when trends are averaged over more and more realizations, the mean trend comes closer and closer to the continuous-limit one. In this sense, the continuous limit is very useful as an indicator of the expected mean trend. On the other hand, the magnitude of the fluctuations seen in any given realization, particularly in certain parts of parameter space, suggest that one should compare the results of a typical realization to observations, in order to get a feel for expected fluctuations in the data from stochastic dynamical processes alone, *i.e.*, apart from those coming from uncertainties in the observational methods of obtaining the data.

Boltzmann approach in its original form appealed to us because of its ability by definition to handle weak, frequent, distant encounters and strong, rare, close encounters on the same footing. Of course, the approach is of practical use only when probabilities or cross-sections of such encounters are known from detailed studies of individual encounters through numerical experiments, as is the case for our current use of this approach. It was generally believed that, since Fokker-Planck methods were normally used for handling only the weak, frequent, distant encounters above, treating their cumulative effect as a diffusion in phase space, this argument would also apply to Monte-Carlo Fokker-Planck methods. However, in a novel feature included recently by Fregeau, Rasio and co-authors (Fregeau et.al 2003; Fregeau & Rasio 2007) in their Monte-Carlo method, both of the above types of encounters are handled in the following way.

The dynamical evolution of the cluster is treated by a basically Hénon-type Monte-Carlo method, which describes this evolution as a sequence of equilibrium models, subject to regular velocity perturbations which are calculated by the standard Hénon method for representing the average effect of many weak, frequent, distant encounters (see Fregeau et.al (2003) and references therein). In addition, the strong, rare, close encounters are by handled by (a) keeping track of the (Monte-Carlo-realized) positions of the objects in the cluster, and so deciding whether two given objects will undergo a strong, close encounter or not, by a *rejection method* very similar to that described above in Sec. 3.1, and then (b) treating these encounters first (i) through cross-sections compiled from analytic fits to numerical scattering experiments (Fregeau et.al 2003), exactly as we have done throughout our approach, and then, (ii) in a more detailed approach, through a direct integration of the strong interaction at hand using standard two- and three-body integrators (Fregeau & Rasio 2007).

A direct comparison of our results with those of above authors is, for the most part, not possible, since we focused primarily on the formation, destruction and hardening of a compact binary population in a given GC environment, while Fregeau et. al focused primarily on the

dynamical evolution of the GC environment in the presence of a given *primordial* binary population. Further, in the latter work, all stars were treated as *point masses* with the *same* mass, as appropriate for a purely cluster-dynamical calculation. However, there is one feature on which we were able to roughly compare our results with those obtained by these and earlier authors. This is the problem of hardening of primordial binaries in GCs, pioneering studies which were performed through direct Fokker-Planck integration by Gao et.al (1991), and through Monte-Carlo method by Hut, McMillan & Romani (1992), and again recently through the above Monte-Carlo method by Fregeau et.al (2003). In an early test run of our scheme, we studied this problem by “turning off” the binary formation and destruction terms in our scheme, thereby studying only the hardening of the primordial binary population through our Boltzmann approach. The results we obtained for the progressive hardening of the binary a -distribution profile (from an initial profile which was uniform in $\ln a$, as in all the above references, and in our work) were, indeed, very similar to those given in the above references.

In a pioneering study, Di Stefano & Rappaport (1992, 1994) explored the tidal-capture formation and subsequent evolution of compact binaries in GCs, concentrating on recycled, millisecond pulsars in the first part of the study (Di Stefano & Rappaport 1992), and on CVs in the second part (Di Stefano & Rappaport 1994). These authors followed the histories of many neutron stars against a given background representing a GC core (parameters corresponding to 47 Tuc and ω Cen were used as typical examples), employing Monte-Carlo methods to generate tidal-capture events in this environment. They followed the subsequent orbital evolution of these binaries due to hardening by gravitational radiation and magnetic braking, until Roche lobe contact occurred. In those cases where such contact occurred through orbit shrinkage before the low-mass companion could reach the giant phase due to its nuclear evolution, these authors did not follow further evolution of the binary, while they did so when the contact occurred due to the evolutionary expansion of the companion.

From the above considerations, Di Stefano and Rappaport estimated the expected number of recycled pulsars and CVs in GCs like 47 Tuc and ω Cen, and also gave the orbital-period distribution of the above binaries at two points, *viz.*, (a) just after tidal capture and orbit circularization, and (b) at Roche-lobe contact. However, their orbital-period distributions cannot be compared directly with those given in this paper (or Paper I) for the following reason. In the Monte-Carlo method of these authors, tidal capture occurs at different times for different binaries, as does Roche-lobe contact. Thus, showing the orbital-period distribution at any of the above two points means, in effect, that the period-distributions at different times are being mixed. By contrast, we have (in this paper and in Paper I) studied the evolution of the orbital period-distribution in time, displaying “snapshots” of the whole distribution at various times, which we called “time slices” above and in Paper I. In our

display, for example, at any given time, some binaries are in Roche-lobe contact and some are not. Indeed, it seems that the orbital period-distributions just after tidal capture, as given by Di Stefano & Rappaport (1992), should be compared with corresponding N-body results given in Portegies Zwart et.al (1997b), and indeed they appear rather similar. We have, of course, pointed out in Paper I, and stress the point here again, that our orbital period-distributions are to be regarded at this stage as intermediate steps in our calculation — rather than final results to be compared with future data on orbital period-distributions of X-ray binaries in GCs — because stellar-evolutionary effects on binary evolution have not been included yet in our scheme (also see below). With this inclusion, the aim would be to produce the GC-analogue of such orbital period-distributions as have been computed by Pfahl et.al. (2003) for LMXBs *outside* GCs.

In addition to the above improvement, we listed in Paper I various other improvements and extensions that are to be implemented in our scheme in future. For example, the compact-binary distribution function above can be looked upon as one obtained by integrating the full, multivariate distribution function which includes other variables, *e.g.*, the binding energy of the binary in the gravitational potential of the GC — the so-called *external* binding energy (or, equivalently, the position of the binary within the GC potential well (Hut, McMillan & Romani 1992)), over these other variables. It would be most instructive to be able to follow the evolution in these additional variables in a more elaborate future scheme.

Encouraged by the veracity of the continuous limit, as presented in this paper, we plan to conclude our program of the first stage of exploration of our Boltzmann scheme by studying one more problem in the same spirit of demonstration of feasibility as we have followed here and in Paper I. This is the question of compact-binary evolution in the environment of an *evolving* GC. Whereas, in keeping with the tradition of numerous previous studies, we have treated the GC environment in Paper I and here as a fixed (*i.e.*, unchanging in time) stellar background, in reality a GC is believed to undergo considerable evolution following the long, quasi-static, “binary-burning” phase, passing through phases of deep core collapse, (possible) gravothermal oscillations, and so on. In this concluding study, we propose to demonstrate that, at the current level of approximation in our scheme, and in the continuous limit, it is possible to follow the evolution of compact-binary populations of GCs through these phases of GC evolution, at the expense of only a modest amount of computing time.

It is a pleasure to thank H. M. Antia, D. Heggie, P. Hut, S. Portegies Zwart, and F. Verbunt for stimulating discussions, and the referee for helpful suggestions.

A. Wiener Processes

Wiener process is the formal mathematical description of Brownian motion — a classic example of a stochastic process, wherein a particle (*e.g.*, pollen grain) on the surface of water undergoes random motion due to stochastic bombardment of it by water molecules. A standard description of the motion such a particle is given by the following differential form due to Langevin:

$$dX_t = a(t, X_t)dt + \sigma(t, X_t)\zeta_t dt. \quad (\text{A1})$$

Here, X_t is one of the components of the particle velocity at time t , and $a(t, X_t)$ is the retarding viscous force. The second term on the right-hand side represents the random molecular force, represented as a product of an intensity factor $\sigma(t, X_t)$ and a random noise factor ζ_t , the latter at each time t being a random number, suitably generated.

A standard Wiener process $W(t)$ is often defined as a continuous Gaussian process with independent increments, satisfying the following properties:

$$W(0) = 0, \quad E(W(t)) = 0, \quad \text{Var}(W(t) - W(s)) = t - s, \quad (\text{A2})$$

for all $0 \leq s \leq t$. Here, E represents the expectation value and ‘Var’ the variance of the indicated stochastic variable⁴. Note that a Wiener process $W_t(\omega)$, can also be thought of as a “pure” Brownian motion with $a = 0$ in Eq. (A1) (Kloeden et.al 1994), wherein the increments $dW_t(\omega)$ for any sample path ω represent a Gaussian white noise.

Eqn. (A1) can then be rewritten in terms of the *symbolic differential* (see below) $dW_s(\omega) \equiv \zeta_s(\omega)ds$ of a Wiener process, and its integral form

$$X_t(\omega) = X_{t_0}(\omega) + \int_{t_0}^t a(s, X_s(\omega))ds + \int_{t_0}^t \sigma(s, X_s(\omega))dW_s(\omega) \quad (\text{A3})$$

represents a path integral over the trajectory of the particle for the sample path $X_t(\omega)$, where ω is a particular trajectory of the Brownian particle.

B. Itô calculus

The problem with the second term on the right-hand side of Eqn. (A3), which represents an integral along a *Wiener path*, is that it is not defined in ordinary calculus, since $W_t(\omega)$

⁴Strictly speaking, the first equation should be written as $W(0) = 0$, w.p.1, where ‘w.p.1’ stands for ‘with probability one’, since we are dealing with random variables here. But we shall not go into mathematical rigor here, referring the reader to Kloeden et.al (1994)

is not differentiable in the ordinary sense. Such an integral along a Wiener path has to be *redefined* suitably to become acceptable mathematically, and the Itô integral is a well-known example of this. The classical limit-of-sum definition of an integral does not hold good for an Itô integral like

$$X_t(\omega) = \int_{t_0}^t f(s, \omega) dW_s(\omega), \quad (\text{B1})$$

since the corresponding finite sum will be divergent over a Wiener path, as sample paths of a Wiener process do not have bounded variance (see above). However, it can be shown that such a sum is *mean-square convergent* under very general conditions (Øksendal 2004), owing to the well-behaved mean-square properties of Wiener processes. Accordingly, Eqn. (B1) is defined only in the sense of *mean-square convergence*, with the result that the integral (B1) is a random variable $X_t(\omega)$ with the following properties:

$$E(X_t) = 0, \quad E(X_t^2) = \int_{t_0}^t E(f(s)^2) ds \quad (\text{B2})$$

Consider now the well-known *Itô formula* for the transformation of a function $f(X_t)$ of a stochastic variable X_t (Gains 1995). For simplicity, first assume that X_t follows a stochastic equation of the form

$$X_t = X_{t_0} + \int_{t_0}^t a(X_t) dt + \int_{t_0}^t \sigma(X_t) dW_t, \quad (\text{B3})$$

i.e., the same as Eqn. (A3), but without explicit time dependence in the continuous and stochastic terms. For brevity, we drop the symbol ω , representing the sample path, in Eqn. (B3) and from here on. Let us divide the entire time span into time-steps at $t_1, t_2, \dots, t_k, \dots$ of length $h_1, h_2, \dots, h_k, \dots$ with the largest step size h_{max} . Then X_t at times t_k and t_{k+1} are related by

$$X_{k+1} = X_k + \int_{t_k}^{t_{k+1}} a(X_t) dt + \int_{t_k}^{t_{k+1}} \sigma(X_t) dW_t, \quad (\text{B4})$$

where we write $X_k \equiv X_{t_k}$ and $X_{k+1} \equiv X_{t_{k+1}}$ for brevity. The Itô formula states (Øksendal 2004) that:

$$f(X_t) = f(X_k) + \int_{t_k}^t \mathcal{L}f(X_s) ds + \int_{t_k}^t f'(X_s) \sigma(X_s) dW_s, \quad (\text{B5})$$

where the operator \mathcal{L} is defined by:

$$\mathcal{L}f(X_s) \equiv f'(X_s)a(X_s) + \frac{1}{2}f''(X_s)\sigma^2(X_s). \quad (\text{B6})$$

For explicitly time-dependent continuous and stochastic terms, the Itô formula can be generalized suitably.

We can use Eqn. (B5) in Eqn. (B4) to expand $a(X_t)$ and $\sigma(X_t)$ around t_k :

$$\begin{aligned} X_{k+1} = & X_k + a(X_k)h_{k+1} + \sigma(X_k)\Delta W_{k+1} \\ & + \int_{t_k}^{t_{k+1}} \int_{t_k}^t \mathcal{L}a(X_s)dsdt + \int_{t_k}^{t_{k+1}} \int_{t_k}^t a'(X_s)\sigma(X_s)dW_sdt \\ & + \int_{t_k}^{t_{k+1}} \int_{t_k}^t \mathcal{L}\sigma(X_s)dsdW_s + \int_{t_k}^{t_{k+1}} \int_{t_k}^t \sigma'(X_s)\sigma(X_s)dW_sdW_t \end{aligned} \quad (\text{B7})$$

Now, if we discard all terms in Eqn. (B7) of $\mathcal{O}(h^\alpha)$ for $\alpha > 1$, we obtain

$$X_{k+1} = X_k + a(X_k)h_{k+1} + \sigma(X_k)\Delta W_{k+1} + \frac{1}{2}\sigma'(X_k)\sigma(X_k) \left((\Delta W_{k+1})^2 - h_{k+1} \right), \quad (\text{B8})$$

which is known as the *Milshtein scheme*. This is the stochastic analogue of the second-order Taylor expansion of ordinary calculus. The Milshtein scheme can be shown to be *strongly* or *pathwise* convergent (Kloeden et.al 1994) to order h , in the sense that the solution converges to the actual Brownian path as $h_{max} \rightarrow 0$. If we restrict the expansion upto the $\mathcal{O}(h^{1/2})$ terms, *i.e.*, upto the first three terms in the right-hand side of (B7), we obtain a slower ($\sim h^{1/2}$) pathwise convergence, which is known as the *Euler-Maruyama scheme*.

For higher dimensions, with $X_k \in \mathcal{R}^{\mathcal{N}}$ and $W_t \in \mathcal{R}^{\mathcal{D}}$, the second-order stochastic Taylor expansion of X_k^i is given by (see Gains (1995) and references therein):

$$X_{k+1}^i = X_k^i + a^i(X_k)h_{k+1} + \sum_{j=1}^{\mathcal{D}} \sigma_j^i(X_k)\Delta W_{k+1}^j + \sum_{j=1}^{\mathcal{N}} \sum_{p,q=1}^{\mathcal{D}} \frac{\partial \sigma_p^i}{\partial X^j} \sigma_q^j(X_k) I_{pq}(k, k+1) + R, \quad (\text{B9})$$

where

$$I_{pq}(k, k+1) \equiv \int_{t_k}^{t_{k+1}} \int_{t_k}^t dW_s^p dW_t^q \quad (\text{B10})$$

and R contains all terms of $\mathcal{O}(h^\alpha)$ for $\alpha > 1$. If $d \leq p, q$ ($p \neq q$), we obtain upon integration by parts:

$$I_{pq}(k, k+1) + I_{qp}(k, k+1) = \Delta W_{k+1}^p \Delta W_{k+1}^q \equiv B_{pq}(k, k+1). \quad (\text{B11})$$

If we further define

$$A_{pq}(k, k+1) \equiv I_{pq}(k, k+1) - I_{qp}(k, k+1), \quad (\text{B12})$$

then we can, with the aid of Eqns. (B12) and (B11), express I_{pq} in terms of A_{pq} and B_{pq} .

Substituting the result in Eqn. (B9), we finally obtain,

$$\begin{aligned}
X_{k+1}^i = & X_k^i + a^i(X_k)h + \sum_p \sigma_p^i(X_k) \Delta W_{k+1}^p \\
& + \frac{1}{2} \sum_{j=1}^{\mathcal{N}} \sum_{p=1}^{\mathcal{D}} \frac{\partial \sigma_p^i}{\partial X^j} \sigma_p^j(X_k) ((\Delta W_{k+1}^p)^2 - h_{k+1}) \\
& + \sum_{j=1}^{\mathcal{N}} \sum_{0 < p < q \leq \mathcal{D}} \frac{1}{2} \left(\frac{\partial \sigma_q^i}{\partial X^j} \sigma_p^j + \frac{\partial \sigma_p^i}{\partial X^j} \sigma_q^j \right) (X_k) B_{pq}(k, k+1) \\
& + \sum_{j=1}^{\mathcal{N}} \sum_{0 < p < q \leq \mathcal{D}} \frac{1}{2} \left(\frac{\partial \sigma_q^i}{\partial X^j} \sigma_p^j - \frac{\partial \sigma_p^i}{\partial X^j} \sigma_q^j \right) (X_k) A_{pq}(k, k+1) + R
\end{aligned} \tag{B13}$$

If $\forall i, p, q$

$$\sum_{j=1}^{\mathcal{N}} \left(\frac{\partial \sigma_q^i}{\partial X^j} \sigma_p^j - \frac{\partial \sigma_p^i}{\partial X^j} \sigma_q^j \right) = 0, \tag{B14}$$

then the A_{pq} terms drop out of Eqn. (B13). Equation (B14) is called the *commutativity condition* and is usually written as,

$$[\sigma_p, \sigma_q] = 0. \tag{B15}$$

When the above commutativity condition is not satisfied, the quantities A_{pq} , known as the *Levy areas*, have to be calculated in order to achieve second-order accuracy.

REFERENCES

- Banerjee, S. and Ghosh, P., 2006, MNRAS, 373, 1188.
- Banerjee, S. and Ghosh, P., 2007, ApJ, 670, 1090 (Paper I).
- Di Stefano, R. and Rappaport, S., 1992, ApJ, 396, 587.
- Di Stefano, R. and Rappaport, S., 1994, ApJ, 423, 274.
- Fabian, A. C., Pringle, J. E. and Rees, M. J. 1975, MNRAS, 172, 15P.
- Fregeau, J. M., Gürkan, M. A., Joshi, K. J. and Rasio, F. A., 2003, ApJ, 593, 772.
- Fregeau, J. M. and Rasio, F. A., 2007, ApJ, 658, 1047.
- Gaines, J.G., 1995, in “Stochastic Partial Differential Equations”, ed. Etheridge, A., Cambridge University Press.

- Gao, B., Goodman, J., Cohn, H. and Murphy, B., 1991, *ApJ*, 370, 567.
- Heggie, D., 1975, *MNRAS*, 173, 729.
- Heggie, D., Hut, P. and McMillan, S.L.W., 1996, *ApJ*, 467, 359.
- Hut, P. and Bahcall, J.N., 1983, *ApJ*, 268, 319.
- Hut, P., McMillan, S. and Romani, R.W., 1992, *ApJ*, 389, 527.
- Kloeden, P.E., Platen, E. and Schurz, H., 1994, “Numerical Solution of SDE Through Computer Experiments”, Springer-Verlag.
- Lee, H.M. and Ostriker, J.P., 1986, *ApJ*, 310, 176.
- Milshtein, G. N., *Th. Prob. Appl.*, 19, 557.
- Øksendal, B., 2004, “Stochastic Differential Equations”, Springer International Edition.
- Pfahl, E.D., Rappaport, S. and Podsiadlowski, P. 2003, *ApJ*, 597, 1036.
- Pooley, D. et.al., 2003, *ApJ*, 591, L131.
- Portegies Zwart, S. F., Hut, P. and Verbunt, F., 1997a, *A&A*, 328, 130.
- Portegies Zwart, S.F., Hut, P., McMillan, S.L.W. and Verbunt, F., 1997b, *A&A*, 328, 143.
- Press, W.H. and Teukolsky, S.A., 1977, *ApJ*, 213, 183.
- Press, W.H., Teukolsky, S.A., Vetterling, W.T., Flannery, B.P., 1992, “Numerical Recipes in C”, Cambridge University Press.
- Shull, J.M., 1979, *ApJ*, 231, 534.
- Sigurdsson, S. and Phinney, E.S., 1993, *ApJ*, 415, 631.
- Spitzer, L. Jr., 1987, “Dynamical Evolution of Globular Clusters”, Princeton Univ. Press.
- Verbunt, F., 2003, in “New Horizons in Globular Cluster Astronomy”, ASP conf. series. 296, 245, eds. G. Piotto et al., Astron. Soc. Pacific, San Francisco.
- Verbunt, F., 2006, in “Highlights of Astronomy”, Volume 14, Proc. XXVIth IAU General Assembly, Prague 2006, ed. van der Hucht, K.A., IAU Publ, Paris.
- Verbunt, F. and Hut, P., 1987, in IAU Symp. 125, “The Origin and Evolution of Neutron Stars”, ed. D. J. Helfand & J. H. Huang, (Dordrecht: Reidel), 187.

Verbunt, F., Lewin, W.G.H and van Paradijs, J. 1989, MNRAS, 241, 51.

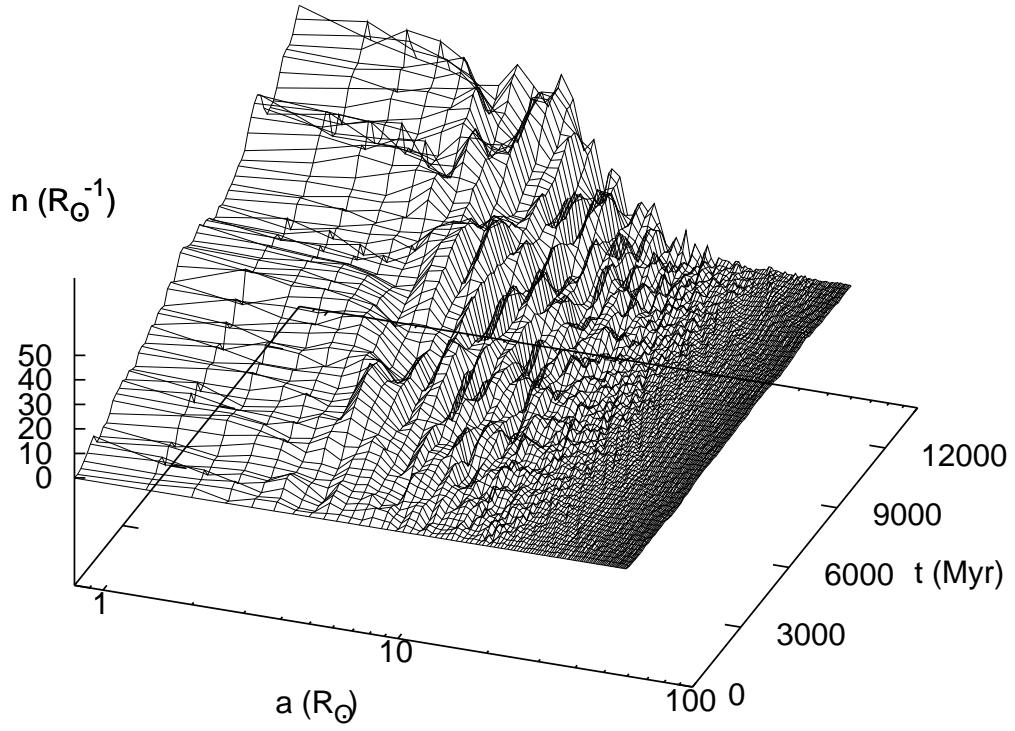


Fig. 1.— A typical example, *i.e.*, one “realization” of the evolution of the binary distribution function $n(a, t)$. Globular cluster parameters are chosen to be roughly those of 47 Tuc, as explained in text (also see Fig. 5 of Paper I).

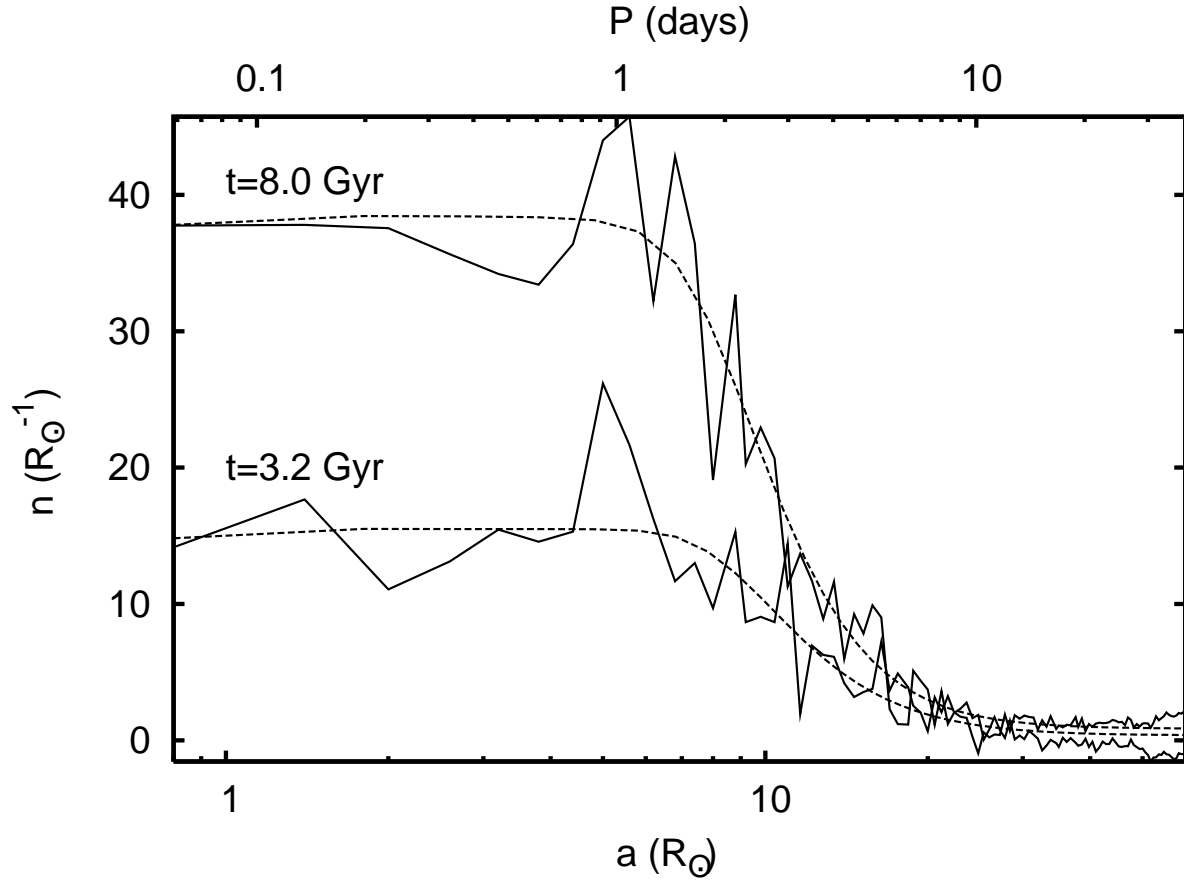


Fig. 2.— Typical time slices, *i.e.*, $n(a)$ at specified times, for the evolution shown in Fig. 1 (solid lines). Overplotted are the same time slices in the continuous limit (dashed lines) from Paper I.

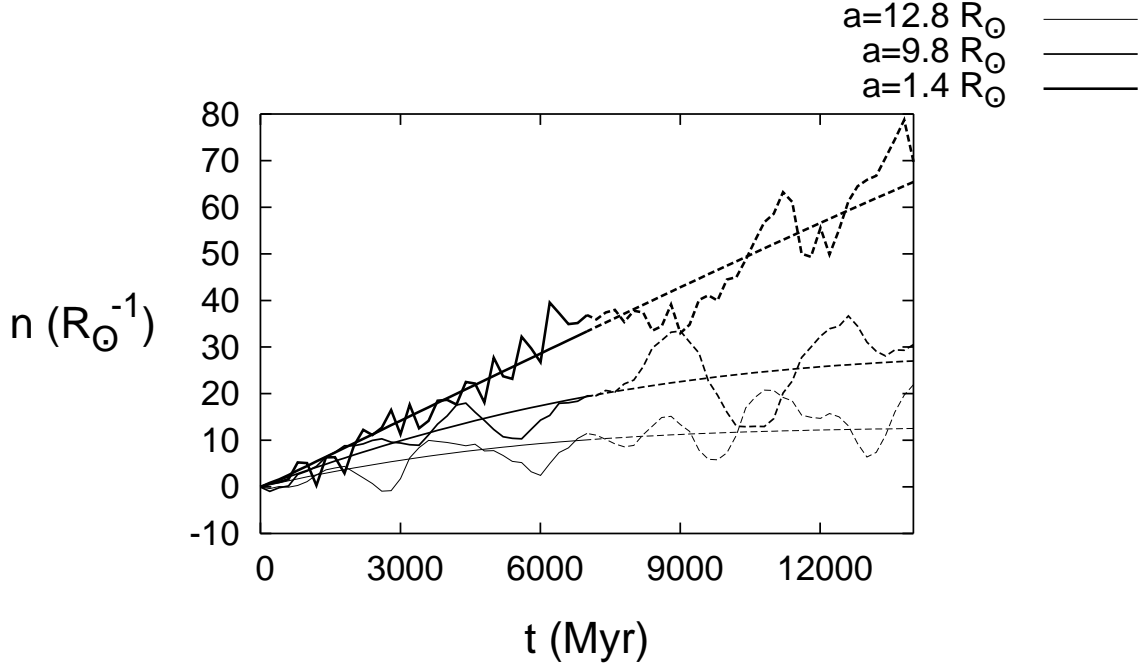


Fig. 3.— Typical radial slices, *i.e.*, $n(t)$ at fixed values of binary radius for the evolution shown in Fig. 1. Overplotted are the same radial slices in the continuous limit from Paper I. As in Paper I, we show the evolution beyond 8 Gyr by dashed lines to indicate that such long evolution times may not be applicable to Galactic GC, but are included here to demonstrate the timescales.

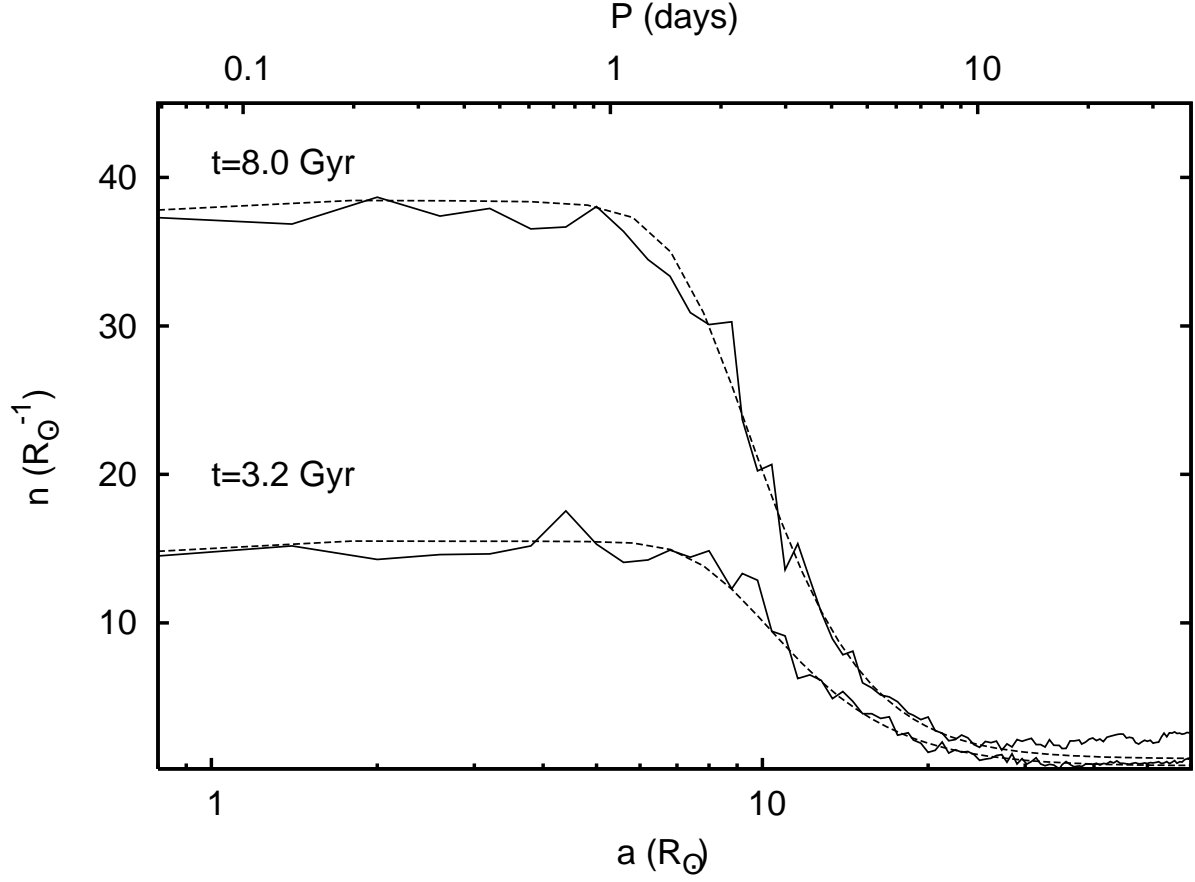


Fig. 4.— Typical time slices through the average evolutionary surface of 12 different “realizations” of the evolution represented in Fig. 1, all with the same GC parameters (solid line). Overplotted are the corresponding time slices in the continuous limit from paper I (dashed line).

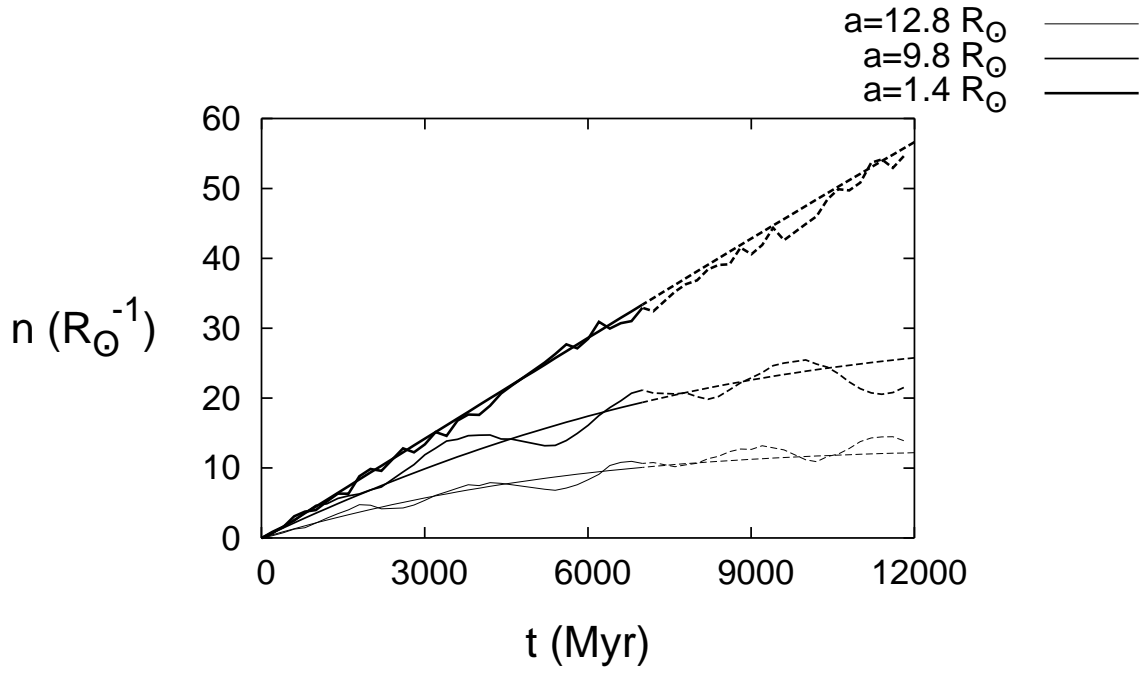


Fig. 5.— Typical radial slices of the same average evolutionary surface as in Fig. 4. Overplotted are the corresponding radial slices in the continuous limit from paper I.

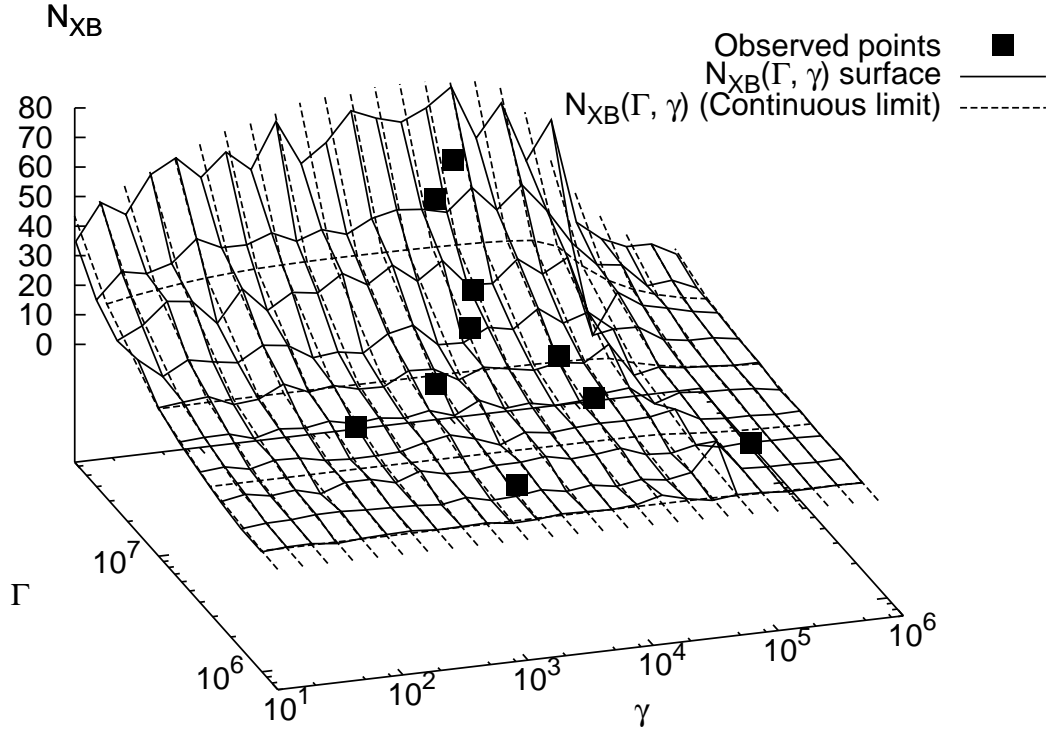


Fig. 6.— $N_{XB}(\gamma, \Gamma)$ surface (solid line). The observed GCs with significant number of XBs are shown overplotted. Also shown overplotted is the continuous-limit result from Paper I (dashed line).

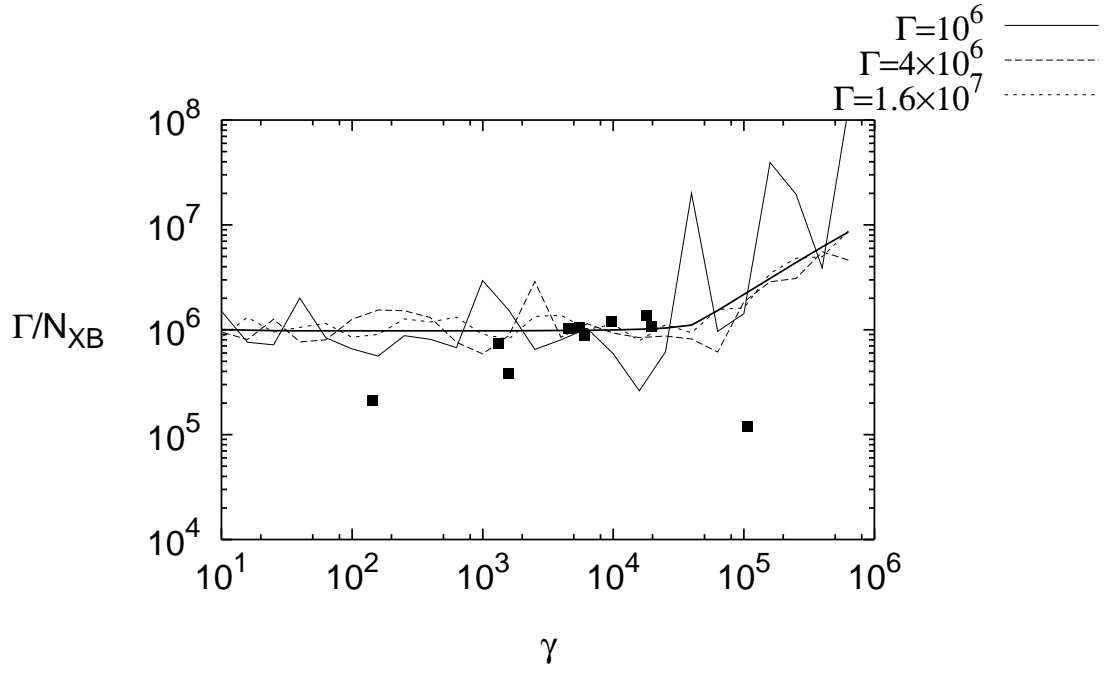


Fig. 7.— Computed Γ/N_{XB} as a function of γ , for values of Γ as indicated. The continuous-limit result for $\Gamma = 10^7$ is shown overplotted (thick line). Also shown overplotted are the positions of Galactic GCs with significant numbers of X-ray sources, as in Paper I.

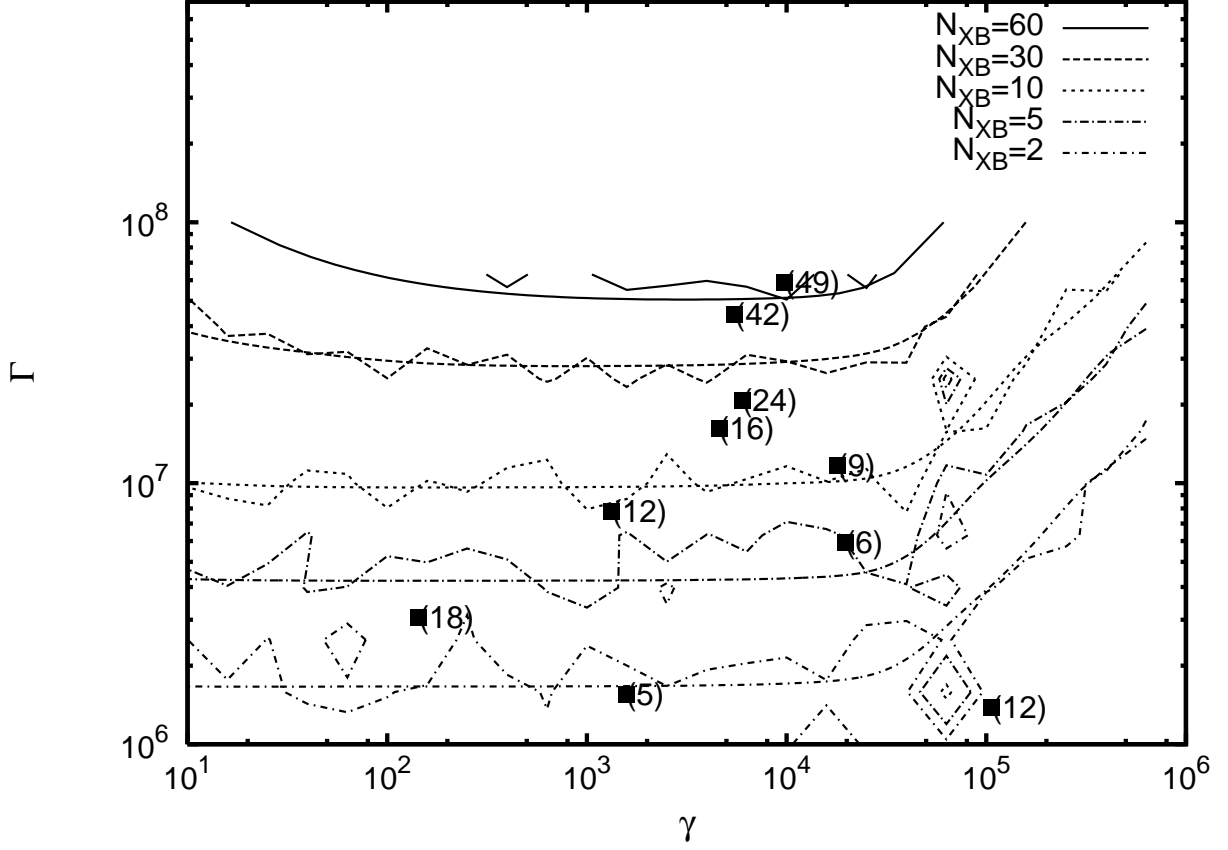


Fig. 8.— Contours of constant N_{XB} in the plane of Verbunt parameters. Corresponding contours in the continuous-limit case are shown overplotted, using the same line-styles for easy comparison. Positions of GCs with significant numbers of X-ray sources are also overplotted, with the corresponding N_{XB} in parentheses, as in Paper I.